



# A thermodynamic condition affecting the movement of a southwest China vortex case

Yongren Chen<sup>1,2,3,4</sup> · Yueqing Li<sup>1,2</sup>

Received: 21 December 2020 / Accepted: 17 February 2022 / Published online: 4 March 2022  
© The Author(s), under exclusive licence to Springer-Verlag GmbH Austria, part of Springer Nature 2022

## Abstract

From 30 June to 5 July 2016, a persistent rainstorm occurred in the Yangtze River basin, China, causing severe floods. This was a rainstorm event associated with a southwest China vortex (SWCV), and four movements of the SWCV were observed. In this paper, we analyze a thermodynamic condition affecting the movement of the SWCV, and the results show that: (1) Equivalent potential temperature could reflect well the thermodynamic variation of the SWCV's movement; thermodynamic structures including distinctive wet–warm (dry–cold) advection in the front (rear) of the SWCV along the direction of motion were important factors for its movement and maintaining the overall cyclonic structure, while dry–cold advection promoted eastward movement of the SWCV. (2) In the four movements of the SWCV, the system existed not only at 700 hPa but also sometimes at 850 hPa. The reasons for this difference lay in the variation of the dry–cold advection in the rear of the SWCV. If the dry–cold advection was located at 700 hPa and above, the cyclonic circulation of the SWCV at 700 hPa was the most complete. The circulation of the 850-hPa SWCV became complete if the dry–cold advection flowed down to 850 hPa and below. Therefore, the synergy between the wet–warm (dry–cold) advection in the front (rear) of the SWCV not only facilitated the movement of the SWCV, but also the maintenance of a complete cyclonic circulation.

## 1 Introduction

Under the interaction between the topography of the Tibetan Plateau and the atmospheric circulation of the region, several different types of precipitating weather systems, with significantly different regional characteristics, frequently form over the body of the Plateau and its surrounding areas. Very early on, Chinese meteorologists pointed out that the eastward development of mesoscale vortices in this region brings heavy rain to downstream areas (Tao and Ding 1981).

For example, the Tibetan Plateau vortex at 500 hPa (Xiang et al. 2013; Yu et al. 2009, 2014, 2016) and the southwest China vortex (SWCV) at 700 hPa and below (Lu 1986; Kuo et al. 1986, 1988; Chen et al. 2015; Chen et al. 2019b; Chen and Li 2021), which, respectively, occur over the Tibetan Plateau and its southeastern side, are the most representative vortex types (Ye and Gao 1979; Lu 1986). In weather charts, an SWCV is described as a mesoscale low vortex, typically originating in southwest China (26°–33°N, 98°–108°E) in the lower troposphere below 700 hPa. Under certain favorable conditions, SWCVs can develop and move eastward to cause flood- and rainstorm-bearing weather. Arguably, SWCVs are the most important precipitation system in the summer half-year, as evidenced by several high-profile events over the past few decades: the occurrence of heavy rain in the Sichuan basin in mid-July 1981 (Kuo et al. 1988); the heavy rainfall and flooding in the Yangtze river in 1998 (Bei et al. 2002; Cheng et al. 2001; Chen et al. 2003); the long-lasting heavy rainfall event that struck south China in mid-June 2008 (Chen et al. 2015); the heavy rainstorms of 8–14 September 2014 (Chen et al. 2019a), 30 June to 1 July 2013 in the eastern part of the Sichuan–Chongqing basin (Cheng et al. 2016), and an abnormal heavy rainfall that occurred on 27 October 2014 in the Sichuan basin (Chen and

Responsible Editor: Clemens Simmer.

✉ Yongren Chen  
yr20060004@163.com

- <sup>1</sup> Institute of Plateau Meteorology, China Meteorological Administration, Chengdu 610072, Sichuan, China
- <sup>2</sup> Heavy Rain and Drought–Flood Disasters in Plateau and Basin Key Laboratory of Sichuan Province, Chengdu 610072, China
- <sup>3</sup> Meteorological Disaster Defense Technology Center of Sichuan Province, Chengdu 610072, Sichuan, China
- <sup>4</sup> Sichuan Provincial Meteorological Observatory, Chengdu 610072, Sichuan, China

Li 2019). All these rainstorm events were associated with an SWCV, indicating the importance of this system for the occurrence of rainstorms and flooding. Thus, the formation, development, and associated floods of SWCVs are hot topics in this field of research.

Scientists researching and working in the fields of meteorology and weather forecasting have carried out numerous studies in which the source region, movement path and types of low vortexes have been analyzed statistically (Chen et al. 2007; Fu et al. 2015). Additionally, there has been much discussion on the structural features of low vortexes and the causes of their formation and development (Wu 1985; Kuo et al. 1986, 1988; Shen et al. 1986; Wang and Orlanski 1987; Wang 1987; Wang et al. 1993; Wang and Tang 2014; Feng et al. 2016; Li et al. 2016), as well as cases studies on the interaction between SWCVs and the Tibetan Plateau Vortex (Li and Deng 2013; Li et al. 2014), encrypted observation experiments (Li and Chen 2015) and numerical simulations (Wang and Gao 2003). However, compared to large-scale low-pressure systems like typhoons and the upper polar vortex, SWCVs are smaller in scale horizontally and shallower in the vertical direction, making them difficult to track and forecast. This limits understanding on the activity of SWCVs, and generates uncertainties and difficulties in predicting their associated rainstorms downstream of the Tibetan Plateau.

In particular, the activity of long-distance SWCVs is especially complicated; the long-distance movement of such SWCVs is not only affected by the environmental wind field (and other weather system activities), but also by the thermodynamic conditions. Against the background of this activity type of southwest China vortex, some past studies have shown SCWVs forming due to the combined effects of topographic features (Wang and Tang 2014). The subtropical high is a key factor in determining the direction of a migratory SWCV, and the steering wind at 700 hPa dominates the direction of SWCV movement (Zhong et al. 2014). Precipitation is a necessary condition for the longevity of an SWCV, and the evolutionary mechanisms and energy characteristics of long-lived SCWVs are typified by significant unevenness (Fu et al. 2015). Yu et al. (2016) revealed some observational facts regarding the joint activities of SWCVs and plateau vortexes, and further pointed out that in most of cases, these two vortexes move eastward together with low troughs. Convective activity moving east from the Tibetan plateau can modify the timing and location of SWCV formation, as well as its displacement (Fu et al. 2019). For a weather system similar the SWCV—the Tibetan plateau vortex—Li et al. (2019) revealed the convergence to the east of 500 hPa Tibetan plateau vortexes, the divergence associated with the westerly jet stream at 200 hPa, and the corresponding ascending motion, provide favorable conditions for the development and eastward movement of the Tibetan plateau

vortexes. However, whilst these studies have discussed the impacts on the movement of SWCVs and their life cycle from the perspective of topography, weather systems and airflow, which are of great help in understanding the activities and development of SWCVs, their emphasis has been limited to the importance of multiscale weather systems and the interaction between airflow and topography. Recently, Chen et al. (2015) revealed that the thermodynamic structures of distinctive warm (cold) advection occurring in the front (rear) of the SWCV's movement are important factors for its evolution—a finding that was important, because it revealed the factors affecting the movement of SWCVs from a new perspective. However, does this thermal structure also exist for other SWCV paths? Is it universal? To reveal the reliability of this thermodynamic structure of SWCV movement, we chose an SWCV case with eastward movement that occurred from 30 June to 5 July 2016 in the Yangtze River Basin.

In this paper, our interest lies in why SWCVs can frequently move eastward to the middle and lower reaches of the Yangtze River. Accordingly, we calculated the pseudo-adiabatic equivalent potential temperature (PEPT) to discuss the factors affecting the movement of this SWCV case. Following this introduction, Sect. 2 describes the data and methods; Sect. 3 describes the activity of the SWCV; Sect. 4 analyzes the thermal structure of the SWCV as it moved eastward; and Sect. 5 concludes the study.

## 2 Data and methods

The data used in this study include:

- (1) Observational data including sounding radio data at 0000 UTC and 1200 UTC, and ground-precipitation data of automatic weather stations (AWSs) provided by the China Meteorological Administration.
- (2) Global final (FNL) Operational Global Analysis data of the National Centers for Environmental Prediction (NCEP), with a spatial resolution of  $1^\circ \times 1^\circ$  and temporal resolution of 6 h, hereafter referred to as NCEP\_fnl (<https://rda.ucar.edu/datasets/ds083.2/>).

As an important thermodynamic parameter, PEPT is taken to be the final temperature which a parcel of air attains when it is lifted dry adiabatically to its lifting condensation level, then pseudo-wet adiabatically (with respect to water saturation) to a great height (dropping out condensed water as it is formed), then finally brought down dry adiabatically to 1000 hPa (Bolton 1980). PEPT has been widely used in meteorological analysis (Hirth et al. 2008; Wu et al. 2011; Hirth et al. 2008; Hurley and Boos 2013; Wahiduzzaman and Yeasmin 2020). To analyze the thermal conditions of

SWCV activity, PEPT and its advection were used to discuss the thermodynamic conditions of the SWCV's movement. According to Davies-Jones (2009) and Zhang (2011), one way to calculate PEPT is as follows:

$$\theta_{se} = T \left( \frac{1000}{p - e} \right)^{R_d / C_{pd}} \exp(L \cdot r / C_{pd} T_c) \quad (1)$$

where  $r = 0.6222e / (p - e)$  is the water vapor mixing ratio,  $T_c$  is the temperature at condensation height,  $e$  is vapor pressure,  $p$  is pressure,  $T$  is temperature,  $L = (2.501 - 0.002370t) \times 10^6 \text{ J} \cdot \text{kg}^{-1}$ , and  $R_d / C_{pd} = 0.2854$ . Therefore,  $\theta_{se}$  is a comprehensive physical quantity that includes temperature, humidity, and pressure, and can reflect the varying characteristics of both moisture and temperature. The term  $-\vec{V} \cdot \nabla \theta_{se}$  is the PEPT advection, wherein if  $-\vec{V} \cdot \nabla \theta_{se} < 0$ , the advection is dry-cold, and if  $-\vec{V} \cdot \nabla \theta_{se} > 0$ , it is wet-warm.

### 3 SWCV movement in a rainstorm event

In a rainstorm event that occurred from 30 June to 5 July 2016 in the Yangtze River Basin, four stages of SWCV activity were observed, as follows: Stage 1, from 0000 UTC 30 June to 1200 UTC 1 July (D1 in Fig. 1), when the vortex circulation built up in the wind fields of 700 hPa and 850 hPa, and the SWCV's activity was concentrated within 30°–31° N; Stage 2, from 1200 UTC 1 July to 0000 UTC 2 July, notable for growth of a new SWCV (D2 in Fig. 1) and during which time the system moved eastward and merged with the old SWCV (D1); Stage 3, from 0000 UTC 2 July to 1200 UTC 3 July, comprising the activity of D3 (the SWCV resulting from the merger of D1 and D2); and Stage 4, from 1200 UTC 3 July, which involved another SWCV

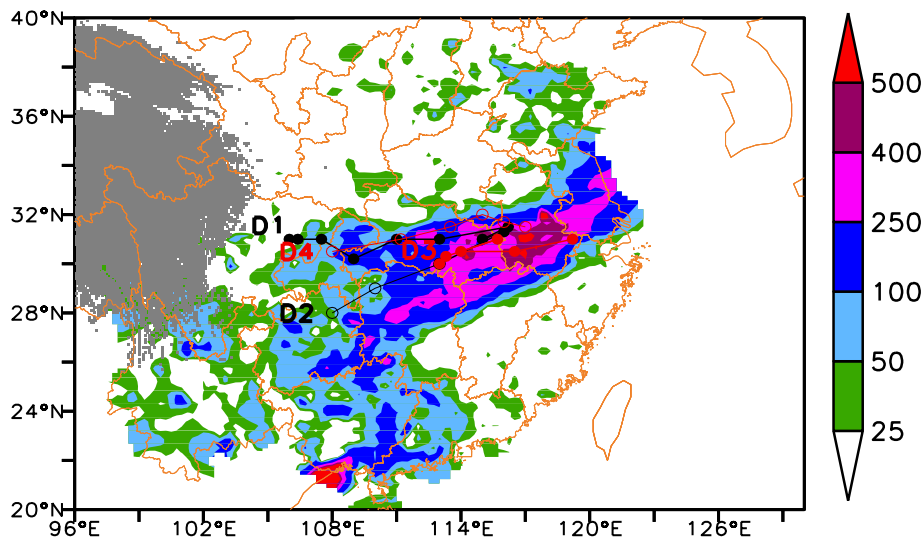
generating near 108°E (D4 in Fig. 1), before then moving eastward to the middle and lower reaches of the Yangtze river, lasting till 1800 UTC 4 July and finally evolving into a shear line. According to the corresponding rainstorm area (colored in Fig. 1), a large-scale rain belt formed along the path of movement of the SWCVs, with the total precipitation amount exceeding 400 mm and the rainstorm area being larger than 500,000 km<sup>2</sup>. This abundance of precipitation led to severe flood-producing rainstorms and associated disasters in the middle and lower reaches of the Yangtze River. Obviously, this is a heavy rain weather process caused by multiple SWCVs that moved eastward and triggered strong precipitation, and the rain belt was highly consistent with the active path.

### 4 Influence of thermal action on SWCV activities

According to the four stages of SWCV activity, D1 began at 0000 UTC 30 July and ended at 1200 UTC 1 July, with a lifespan of 36 h. D2, whose vortex circulation was reflected at 700–850 hPa, generated near 108°E and lasted only 12 h, from 1200 UTC 1 July to 0000 UTC 2 July. At 0000 UTC 2 July, D1 merged with D2 to form D3, and then disappeared at 1200 UTC 3 July. At the same time, D4 generated, and its circulation lasted till 0000 UTC 5 July.

To analyze the thermodynamic influence on the movement of this SWCV system, Figs. 2 and 3 show the circulation of D1–D4 and the distribution of  $-\vec{V} \cdot \nabla \theta_{se}$  at 700 hPa and 850 hPa, respectively. As demonstrated by Figs. 2a–d and 3, a–d, D1 started to generate in the region of 105°E at 0000 UTC 30 June, and ended at 1200 UTC 1 July, with a lifespan of 36 h. During this phase, a thermodynamic structure involving wet-warm (dry-cold) advection in the

**Fig. 1** Distribution of the SWCV's path based on NCEP\_fnl data every 6 h from 0000 UTC 30 June to 0000 UTC 5 July 2016, along with the observed accumulated precipitation (color-shaded; unit: mm). D1: path of the SWCV in stage 1; D2: path of the SWCV in stage 2; D3: path of the SWCV in stage 3; D4: path of the SWCV in stage 4



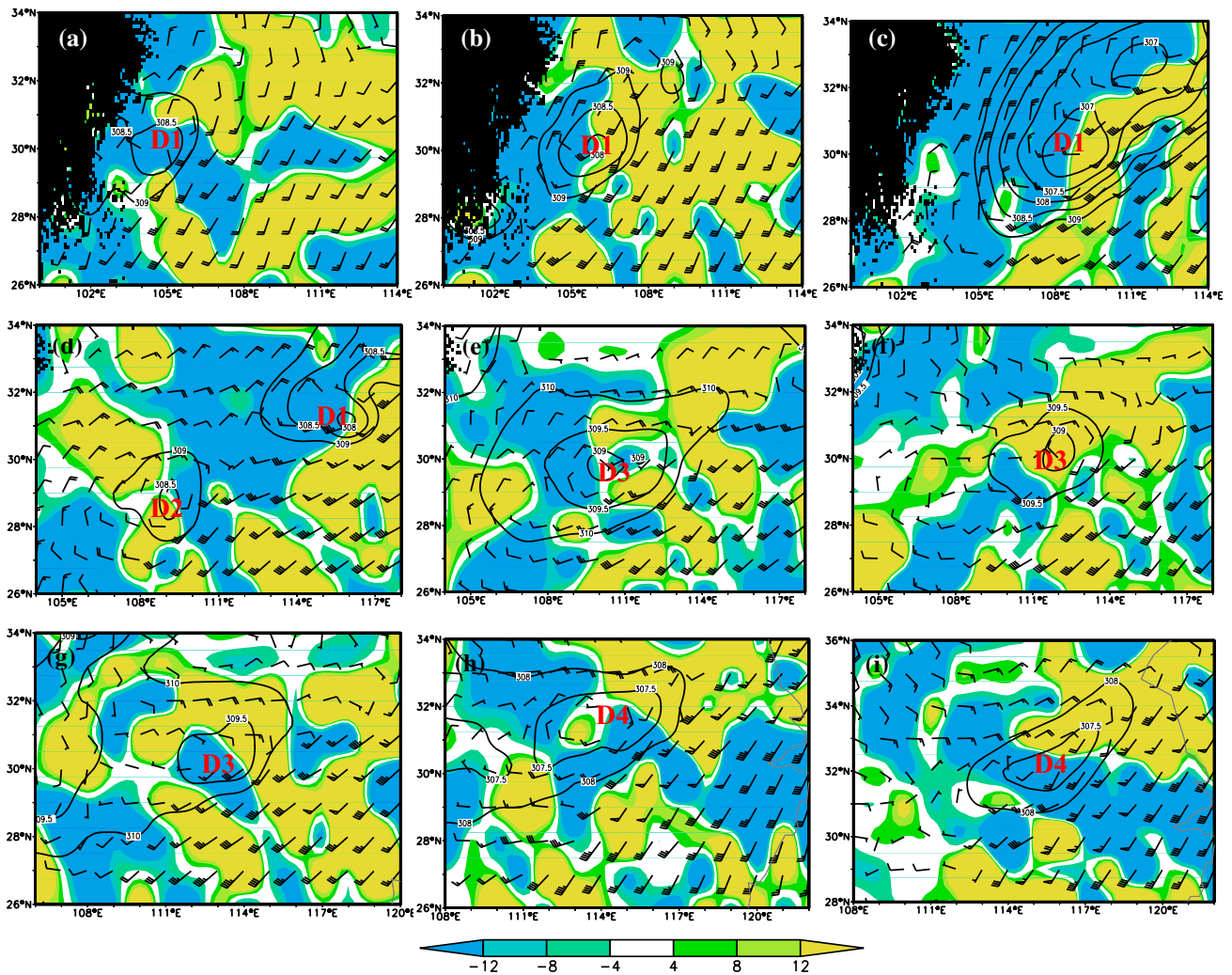


**Fig. 2** The wind vector (unit:  $\text{m s}^{-1}$ ), geopotential height (contours; unit:  $\text{gpdam}$ ), and distribution of  $-\vec{V} \cdot \nabla\theta_{se}$  (shaded; unit:  $10^{-5} \text{K s}^{-1}$ ) at 700 hPa, at (a) 0000 UTC 30 June, (b) 0600 UTC 30 June, (c)

1800 UTC 30 June, (d) 1200 UTC 1 July, (e) 0000 UTC 2 July, (f) 0600 UTC 2 July, (g) 1200 UTC 2 July, (h) 0000 UTC 4 July, and (i) 0600 UTC 4 July

front (rear) of the SWCV was found. With time, the range of the dry–cold advection expanded and the SWCV gradually moved eastward. At 0600 UTC 30 June, the SWCV moved to  $107^\circ \text{E}$ , and reached  $110^\circ \text{E}$  at 1200 UTC 30 June and  $115^\circ \text{E}$  at 1200 UTC 1 July.

At the same time (1200 UTC 1 July), another SWCV (D2) formed, located over the region  $106^\circ\text{--}108^\circ \text{E}$ , with a lifespan of only 12 h (Figs. 2d, 3d). In this phase, a structure involving wet–warm (dry–cold) advection in the front (rear) of the SWCV was also found at 700 hPa, but not so obviously at 850 hPa. However, the thermodynamic characteristic of D2's center differed between 700 and 850 hPa, with wet–warm (dry–cold) advection at 700 hPa (850 hPa).

Up until 0000 UTC 2 July, a process took place by which D1 merged with D2 to form D3, which was located over the region  $108^\circ\text{--}110^\circ \text{E}$ . D3's activity lasted about 36 h, from

0000 UTC 2 July to 1200 UTC 3 July, and its lifespan was longer. During its period of movement, there was an obvious thermodynamic structure involving wet–warm (dry–cold) advection in the front (rear); and influenced by the cold advection, D3 moved eastward to  $112^\circ \text{E}$  at 0600 UTC 2 July, and then to  $114^\circ \text{E}$  at 1200 UTC 2 July. Starting from 0600 UTC 3 July, the warm advection strengthened further, but the cold advection weakened, meaning D3 itself gradually weakened too. At 1200 UTC 3 July, D3 disappeared and the third stage of activity ended.

In the fourth stage of activity, the movement of D4 lasted about 30 h. In Figs. 2h, i, and 3h, i, it is also apparent that the thermodynamic structure involving wet–warm (dry–cold) advection existed in the front (rear) of D4. Thus, the complete cyclonic circulation of the SWCV still maintained this same structure during its movement, and the enhancement

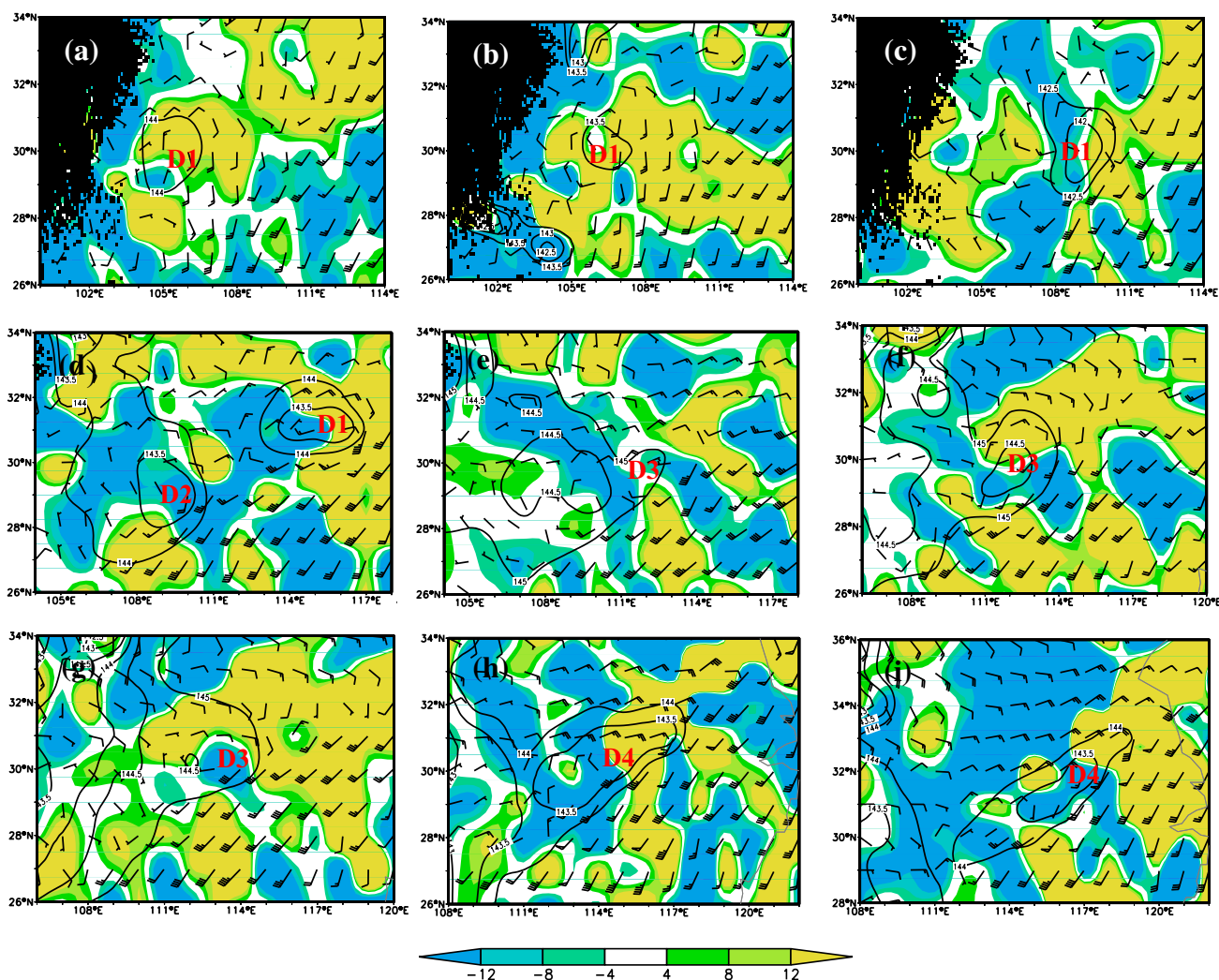


Fig. 3 As in Fig. 2, but for 850 hPa

of the dry–cold advection helped to promote the movement of the SWCV to the wet–warm advection zone. Therefore, we conclude that this thermal structure was crucial to the SWCV’s activity.

However, the above analysis focuses only on the horizontal direction. What about the thermal structure in the variation of the vertical profile? Figs. 4, 5 show the profiles along the direction of movement of the SWCV, demonstrating clearly that the dry–cold and wet–warm advection was very deep.

During the movement of D1 (Fig. 4), the front of D1 was always characterized by wet–warm advection, and the rear by dry–cold advection. Also, the vortex center was located near the advection zero line. For example, at 0000 UTC 30 June, the wet–warm advection of the SWCV’s front was stronger than the dry–cold advection of the SWCV’s rear; the former existed in the entire atmospheric layer (from nearly the surface to 250 hPa), and the latter was distributed

above 800 hPa and was weak. Up until 0600 UTC 30 June, the dry–cold advection of D1’s rear enhanced and its scope expanded, and at the same time, the vortex moved near to 106°E. By 1200 UTC 30 June, the range of dry–cold advection had expanded significantly, and D1 continued to move eastward. Up until 1800 UTC 1 July, the dry–cold advection expanded to 109° E and, correspondingly, the center of D1 was located near 109° E. By 0000 UTC 1 July, D1 had moved to 113°E, and then to 116°E at 1200 UTC 1 July.

In phases D2–D4, when the various vortex mergers took place (Fig. 5), a thermodynamic structure involving wet–warm (dry–cold) advection in the front (rear) of D1 and D4 (Fig. 5a, b) existed at 1800 UTC 01 July, by which time D1 had moved slightly toward the southwest and D2 toward the northeast. At 0000 UTC 2 July, D3 formed by the merger of D1 and D2 and, influenced by dry–cold advection, continued to move eastward (Fig. 5c–e). At 1200 UTC 2 July, D3 moved to 114°E, and at 0000 UTC 3 July it moved to 116°E

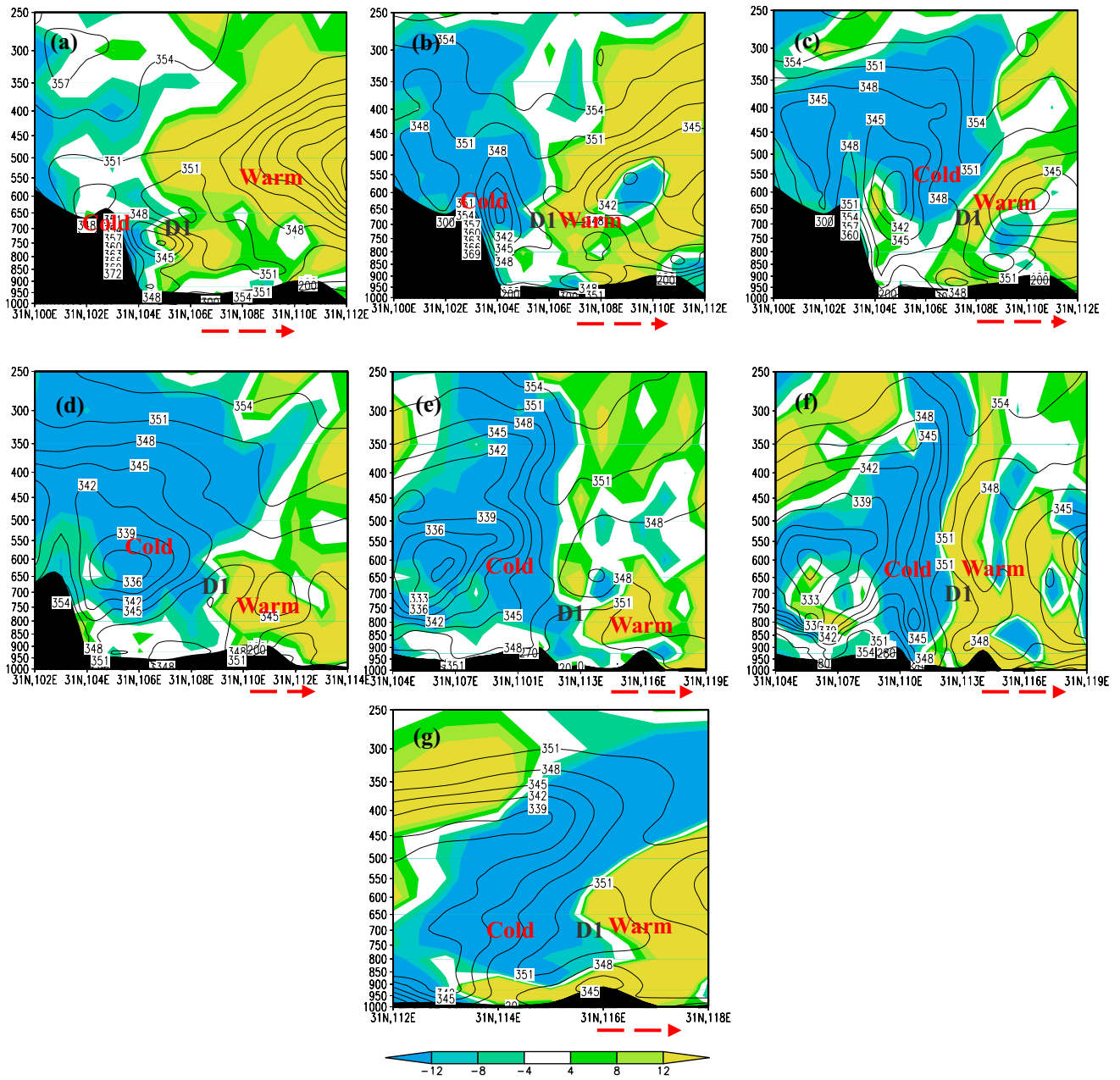


**Fig. 4** Distribution of  $-\vec{V} \cdot \nabla \theta_{se}$  (shaded; unit:  $10^{-5} \text{ K s}^{-1}$ ) and  $\theta_{se}$  (contours; unit: K) for the movement of D1 at (a) 0000 UTC 30 June,

(b) 0600 UTC 30 June, (c) 1200 UTC 30 June, (d) 1800 UTC 30 June, (e) 0000 UTC 1 July, (f) 0600 UTC 1 July, and (g) 1200 UTC 1 July. The red arrow indicates the direction of SWCV movement

and 118°E. In terms of D4’s activity—the last stage of the rainstorm—this began from 0000 UTC 4 July. The dry–cold advection in the rear of D1 strengthened and D4 gradually moved to the wet–warm advection zone. The thermal structure involving wet–warm (dry–cold) advection in the front (rear) of D4 became more obvious and lasted till 1800 UTC 4 July. By 0000 UTC 5 July, this thermal structure had disappeared and D4’s activity gradually came to an end. Therefore, from these results, we can again see the importance of

the synergistic effect of dry–cold and wet–warm advection on the movement of SWCVs.

### 5 Conclusions and discussion

Using PEPT to calculate the advection, the thermal conditions of four SWCV movements during a persistent heavy-rain event in the Yangtze River basin, from 30 June to 5

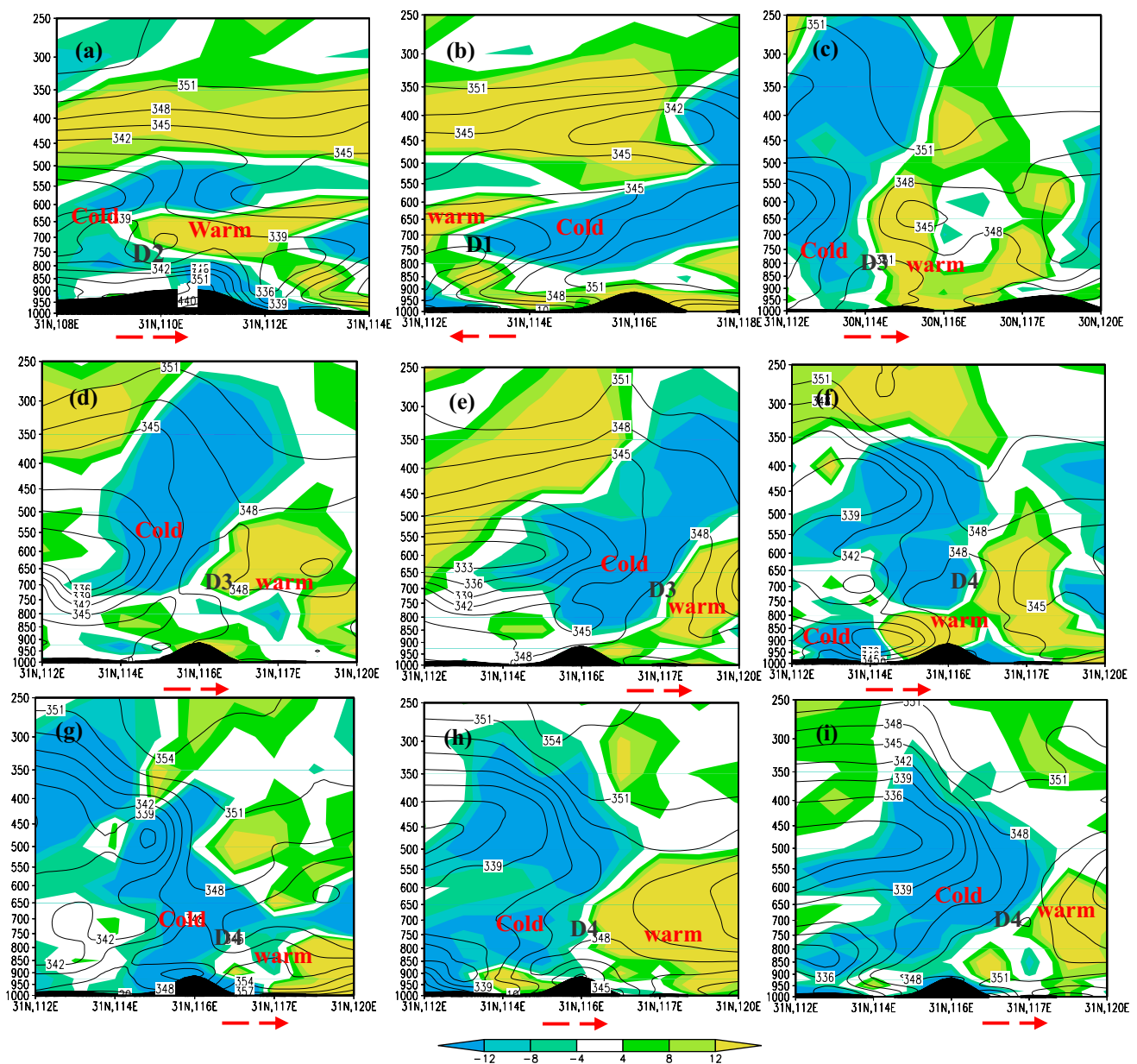


**Fig. 5** As in Fig. 4, but for the movement of D2, D3 and D4 at (a, b) 1800 UTC 1 July, (c) 1200 UTC 2 July, (d) 1800 UTC 2 July, (e) 0000 UTC 3 July, (f) 0000 UTC 4 July, (g) 0600 UTC 4 July, (h)

1200 UTC 4 July, and (i) 1800 UTC 4 July. The red arrow indicates the direction of SWCV movement

July 2016, are discussed, and the synergistic influence of the wet–warm (dry–cold) advection on the SWCV movement is further revealed. The main conclusions are as follows:

(1) This was a case of SWCV activity with an eastward path, and its movement was closely related to dry–cold advection at its rear. During the four movements, the enhancement of this rear dry–cold advection continually drove the vortices to the wet–warm advection zone, which

was not only reflected in the horizontal direction, but also the vertical.

(2) The structure of the wet–warm (dry–cold) in the front (rear) part of the SWCV was one of the thermal conditions necessary for maintaining the overall cyclonic circulation. Generally, when the structure of dry–cold and wet–warm advection in the near-vortex areas became more obvious, the cyclonic structure of the SWCV was more complete. In addition, the entire vortex appeared at 700 hPa and 850 hPa, but sometimes only in a single level, which was also related to the effect of the dry–cold advection in the vertical direc-

tion. If the dry–cold advection affected 700 hPa and above, the SWCV had its most complete cyclonic circulation at 700 hPa; whereas, if the dry–cold advection affected 850 hPa and below, the SWCV circulation at this level became more complete. Therefore, the synergy of wet–warm (dry–cold) in the front (rear) part of the SWCV not only facilitated its movement, but also the maintenance of a complete cyclonic circulation. This further validates the importance of thermodynamic advection for the movement and maintenance of SWCVs.

(3) It is important to note that this was a typical mesoscale vortex whose formation was related to the combined effects of the topography. Most vortices are mainly located over the Sichuan basin, which is known within China for its high level of incidence regarding torrential rain and flooding, and rarely move over long distances. For the conditions of SWCVs movement, past studies discussed it from the perspectives of topography, weather systems and airflow, which are of great help in understanding the activities and development of SWCV, but mainly emphasized the importance of multi-scale weather systems and interaction between airflow and topography. In the present study, we revealed the importance of structure of the wet–warm (dry–cold) advection to the movement of the SWCV, however, the present study is limited by the sample size, and more cases are needed for further validation, in particular how to define a criterion for cold advection steering the movement of SWCV, these topics further deserve to be researched.

**Acknowledgements** This work was jointly sponsored by the National Natural Science Foundation of China (No.91937301), Sichuan Science and Technology Program (2021YFS0326); the National Natural Science Foundation of China (No.42030611), a key project of the National Natural Science Foundation of China (No. 42030611), the Scientific and Technological Research Program of China Railway Eryuan Engineering Group CO.LTD (No.KYY2020066(20-22) ), a Strategic Priority Research Program of Chinese Academy of Sciences (No. XDA23090103), and a special project of the forecaster of China Meteorological Administration (CMAYBY2020-113).

**Data availability** (1) Sounding observational data, and land surface precipitation data are from observational systems of China Meteorological Administration. The datasets generated during and/or analyzed during the current study are available from the corresponding author on reasonable request. (2) Global final (FNL) analysis data from the National Centers for Environmental Prediction (NCEP), with a spatial resolution of  $1 \times 1$  and temporal resolution of 6 h (hereafter referred to as NCEP\_fnl data); the data can be freely downloaded from the link <https://rda.ucar.edu/datasets/ds083.2/>.

## Declarations

**Conflict of interest** The authors declare that there are no conflicts of interest regarding the publication of this paper.

## References

- Bei NF, Zhao SX, Gao ST (2002) Numerical simulation of a heavy rainfall event in China during July 1998. *Meteorol Atmos Phys* 80:153–164. <https://doi.org/10.1007/s007030200022>
- Bolton D (1980) The computation of equivalent potential temperature. *Mon Wea Rev* 108:1046–1053. [https://doi.org/10.1175/1520-0493\(1980\)108%3c1046:TCOEPT%3e2.0.CO;2](https://doi.org/10.1175/1520-0493(1980)108%3c1046:TCOEPT%3e2.0.CO;2)
- Chen YR, Li YQ (2019) Analysis of a late-autumn rainstorm in the Sichuan basin on the eastern side of the Tibetan Plateau. *Adv Meteorol*. <https://doi.org/10.1155/2019/8797368>
- Chen YR, Li YQ (2021) Convective characteristics and formation conditions in an extreme rainstorm on the eastern edge of the Tibetan plateau. *Atmosphere* 12:381. <https://doi.org/10.3390/atmos12030381>
- Chen LS, Luo ZX (2003) A preliminary study of the dynamics of eastward shifting cyclonic vortices. *Adv Atmos Sci* 20:323–332. <https://doi.org/10.1007/BF02690790>
- Chen QZ, Huang YW, Wang QW, Tan ZM (2007) The statistical study of the southwest vortex during 1990–2004. *J Nanjing Univ* 43(6):633–642 (in Chinese)
- Chen YR, Li YQ, Zhao TL (2015) Cause analysis on eastward movement of southwest China vortex and its induced heavy rainfall in south China. *Adv Meteorol*. <https://doi.org/10.1155/2015/481735>
- Chen YR, Li YQ, Qi DM (2019a) Analysis of the convective characteristics during the mutual evolution of an inverted trough/low vortex and its induced rainstorm over the northeastern Sichuan basin, China. *Meteorol Atmos Phys* 131:807–825. <https://doi.org/10.1007/s00703-018-0607-4>
- Chen YR, Li YQ, Kang L (2019b) An index reflecting mesoscale vortex–vortex interaction and its diagnostic applications for rainstorm area. *Atmos Sci Lett* 20:e902. <https://doi.org/10.1002/asl.902>
- Cheng MH, He HZ, Mao DY, Qi YJ, Cui ZH, Zhou FX (2001) Study of 1998 heavy rainfall over the Yangtze river basin using TRMM data. *Adv Atmos Sci* 18:387–396. <https://doi.org/10.1007/BF02919317>
- Cheng XL, Li YQ, Xu L (2016) An analysis of an extreme rainstorm caused by the interaction of the Tibetan Plateau vortex and the southwest China vortex from an intensive observation. *Meteorol Atmos Phys* 128:373–399. <https://doi.org/10.1007/s00703-015-0420-2>
- Davies-Jones R (2009) On formulas for equivalent potential temperature. *Mon Wea Rev* 137:3138–3147. <https://doi.org/10.1175/2009MWR2774.1>
- Feng XY, Liu CH, Fang GZ, Liu XD, Fang CY (2016) Climatology and structures of southwest vortices in the NCEP climate forecast system reanalysis. *J Clim* 29:7675–7701. <https://doi.org/10.1175/JCLI-D-15-0813.1>
- Fu SM, Li WL, Sun JH, Zhang JP, Zhang YC (2015) Universal evolution mechanisms and energy conversion characteristics of long-lived mesoscale vortices over the Sichuan basin. *Atmos Sci Lett* 16:127–134. <https://doi.org/10.1002/asl2.533>
- Fu SM, Mai M, Sun JH, Wan LL, Ding Y, Wang YQ (2019) Impacts of convective activity over the Tibetan plateau on plateau vortex, southwest vortex, and downstream precipitation. *J Atmos Sci* 76:3803–3830. <https://doi.org/10.1175/JAS-D-18-0331.1>
- Hirth BD, Schroeder JL, Weiss CC (2008) Surface analysis of the rear-flank downdraft outflow in two tornadic supercells. *Mon Wea Rev* 136:2344–2363. <https://doi.org/10.1175/2007MWR2285.1>
- Hurley JV, Boos WR (2013) Interannual variability of monsoon precipitation and local subcloud equivalent potential temperature. *J Clim* 26:9507–9527. <https://doi.org/10.1175/JCLI-D-12-00229.1>
- Kuo YH, Cheng LS, Anthes RA (1986) Mesoscale analyses of the Sichuan flood catastrophe, 11–15 July 1981. *Mon Weather Rev*



- 114:1984–2003. [https://doi.org/10.1175/1520-0493\(1986\)114%3C1984:MAOTSF%3E2.0.CO;2](https://doi.org/10.1175/1520-0493(1986)114%3C1984:MAOTSF%3E2.0.CO;2)
- Kuo YH, Cheng LS, Bao JW (1988) Numerical simulation of the 1981 Sihan flood. Part I: evolution of a mesoscale southwest vortex. *Mon Wea Rev* 116:2481–2504. [https://doi.org/10.1175/1520-0493\(1988\)116%3c2481:NSOTSF%3e2.0.CO;2](https://doi.org/10.1175/1520-0493(1988)116%3c2481:NSOTSF%3e2.0.CO;2)
- Li G, Deng J (2013) Atmospheric water monitoring by using ground-based GPS during heavy rains produced by TPV and SWV. *Adv Meteorol*. <https://doi.org/10.1155/2013/793957>
- Li J, Du J, Zhang DL, Cui CG, Liao YS (2014) Ensemble-based analysis and sensitivity of mesoscale forecasts of a vortex over southwest China. *Quart J Roy Meteor Soc* 140:766–782. <https://doi.org/10.1002/qj.2200>
- Li YQ, Yu L, Chen BD (2015) An assessment of design of observation network over the Tibetan Plateau based on observing system simulation experiments (OSSE). *J Meteorol Soc Japan* 93:343–358. <https://doi.org/10.2151/jmsj.2015-019>
- Li N, Ran LK, Gao ST (2016) The impact of deformation on vortex development in a baroclinic moist atmosphere. *Adv Atmos Sci* 33:233–246. <https://doi.org/10.1007/s00376-015-5082-y>
- Li L, Zhang RH, Min W, Duan JP (2019) Development and eastward movement mechanisms of the Tibetan plateau vortices moving off the Tibetan plateau. *Clim Dyn* 52:4849–4859. <https://doi.org/10.1007/s00382-018-4420-z>
- Lu JH (1986) Generality of the southwest vortex. China meteorological press, Beijing: 1–276 (in Chinese)
- Shen RJ, Reiter ER, Bresch JF (1986) Numerical simulation of the development of vortices over the Qinghai-Xizang Plateau. *Meteorol Atmos Phys* 35:70–95. <https://doi.org/10.1007/BF01029526>
- Tao SY, Ding YH (1981) Observational evidence of the influence of the Qinghai-Xizang (Tibet) Plateau on the occurrence of heavy rain and severe convective storms in China. *Bull Amer Meteor Soc* 62:23–30. [https://doi.org/10.1175/1520-0477\(1981\)062%3c0023:OEOTIO%3e2.0.CO;2](https://doi.org/10.1175/1520-0477(1981)062%3c0023:OEOTIO%3e2.0.CO;2)
- Wahiduzzaman M, Yeasmin A (2020) A kernel density estimation approach of north Indian ocean tropical cyclone formation and the association with convective available potential energy and equivalent potential temperature. *Meteorol Atmos Phys* 132:603–612. <https://doi.org/10.1007/s00703-019-00711-7>
- Wang B (1987) The development mechanism for Tibetan Plateau warm vortices. *J Atmos Sci* 44:2978–2994. [https://doi.org/10.1175/1520-0469\(1987\)044%3c2978:TDMFTP%3e2.0.CO;2](https://doi.org/10.1175/1520-0469(1987)044%3c2978:TDMFTP%3e2.0.CO;2)
- Wang Z, Gao K (2003) Sensitivity experiments of an eastward-moving southwest vortex to initial perturbations. *Adv Atmos Sci* 20:638–649. <https://doi.org/10.1007/BF02915507>
- Wang B, Orlanski I (1987) Study of a heavy rain vortex formed over the eastern flank of the Tibetan Plateau. *Mon Wea Rev* 115:1370–1393. [https://doi.org/10.1175/1520-0493\(1987\)115%3c1370:SOAHRV%3e2.0.CO;2](https://doi.org/10.1175/1520-0493(1987)115%3c1370:SOAHRV%3e2.0.CO;2)
- Wang QW, Tan ZM (2014) Multi-scale topographic control of southwest vortex formation in Tibetan Plateau region in an idealized simulation. *JGR Atmos* 119:11543–11561. <https://doi.org/10.1002/2014JD021898>
- Wang W, Kuo YH, Warner TT (1993) A diabatically driven mesoscale vortex in the lee of the Tibetan Plateau. *Mon Wea Rev* 121:2542–2561. [https://doi.org/10.1175/1520-0493\(1993\)121%3c2542:ADDMVI%3e2.0.CO;2](https://doi.org/10.1175/1520-0493(1993)121%3c2542:ADDMVI%3e2.0.CO;2)
- Wu GX, Chen SJ (1985) The effect of mechanical forcing on the formation of a mesoscale vortex. *Quart J Roy Meteor Soc* 111:1049–1070. <https://doi.org/10.1002/qj.49711147009>
- Wu XD, Ran LK, Chu YL (2011) Diagnosis of a moist thermodynamic advection parameter in heavy-rainfall events. *Adv Atmos Sci* 28:957–972. <https://doi.org/10.1007/s00376-009-9057-8>
- Xiang SY, Li YQ, Li D, Yang S (2013) An analysis of heavy precipitation caused by a retracing plateau vortex based on TRMM data. *Meteorol Atmos Phys* 122:33–45. <https://doi.org/10.1007/s00703-013-0269-1>
- Ye DZ, Gao YX (1979) Meteorology of the Tibetan Plateau. China Scientific Press, Beijing, pp 1–278
- Yu SH, Gao WL (2009) Large-scale conditions of Tibet Plateau vortex departure. *Sci Cold and Arid Reg* 1:559–569
- Yu SH, Gao WL, Peng J, Xiao YH (2014) Observational facts of sustained departure Plateau vortices. *J Meteor Res* 28:296–307. <https://doi.org/10.1007/s13351-014-3023-9>
- Yu SH, Gao WL, Xiao DX, Peng J (2016) Observational facts regarding the joint activities of the southwest vortex and plateau vortex after its departure from the Tibetan Plateau. *Adv Atmos Sci* 33:34–46. <https://doi.org/10.1007/s00376-015-5039-1>
- Zhang GC (2011) Analysis and prediction of strong convective weather. China Meteorological Press, Beijing, pp 58–60
- Zhong R, Zhong LH, Hua LJ, Feng SD (2014) A climatology of the southwest vortex during 1979–2008. *Atmos Oceanic Sci Lett* 6:577–583. <https://doi.org/10.3878/AOSL20140042>

**Publisher's Note** Springer Nature remains neutral with regard to jurisdictional claims in published maps and institutional affiliations.